In-depth analysis and evaluation of diffusive glioma models

A. Roniotis, V. Sakkalis, I. Karatzanis, M. Zervakis, *Member, IEEE* and K. Marias, *Member, IEEE*

***Abstract*— Glioma is one of the most aggressive types of brain tumor. Several mathematical models have been developed during the last two decades, towards simulating the mechanisms that govern the development of glioma. The most common models use the diffusion-reaction equation (DRE) for simulating the spatiotemporal variation of tumor cell concentration. Nevertheless, despite the applications presented, there has been little work on studying the details of the mathematical solution and implementation of the 3D diffusion model and presenting a qualitative analysis of the algorithmic results. This paper presents a complete mathematical framework on the solution of the DRE using different numerical schemes. This framework takes into account all characteristics of the latest models, such as brain tissue heterogeneity, anisotropic tumor cell migration, chemotherapy and resection modeling. The different numerical schemes presented have been evaluated based upon the degree to which the DRE exact solution is approximated. Experiments have been conducted both on real datasets and a test case for which there is a known algebraic expression of the solution. Thus, it is possible to calculate the accuracy of the different models.**

keywords*: computational oncology, cancer modeling, glioblastoma, diffusion reaction equation*

I. Introduction

GLIOMA is the most malignant form of brain tumor, which exhibits a highly invasive behavior against neighboring tissue. Glioma is characterized by poor detection of the tumor boundaries by the common imaging techniques (MRI, CT, PET). Since early 90s, researchers have proposed several approaches for the development of models that can simulate the procedure of glioma growth. Such models facilitate the visualization of the exact tumor boundaries and the prediction of tumor expansion. Moreover, models that incorporate therapy parameters could be used for optimizing therapy results, since radiologists could predict the response of the patient to different therapeutic schemes.

The most common models employ variations of the diffusion – reaction equation in order to simulate the spatiotemporal change of tumor cell density. However, the various implementations of diffusive models for gliomas lack a firm presentation of the mathematical background on the derivation and solution of the equation. Moreover, the plethora of numerical methods used in the solution raise the crucial question on how these implementation methods compare to each other. The main contribution of this paper is a detailed mathematical framework of a modern diffusive model for glioma using several numerical methods and more importantly, an in-depth comparative study between different implementations aiming to serve as a reference for modelers in this field. To this end, it stresses the limitations and advantages of each modeling scheme by providing quantitative comparison that can be crucial for translating such models in the clinical setting. Besides the development of a generic model in section II, the paper proceeds with the elaboration on numerical methods in section III, based on finite elements and finite difference approaches. The implementation of methods is tested and compared on real glioma cases, as presented in section IV. The analysis of algorithmic results and comparisons are presented in sections V and VI for finite differences and finite elements, respectively. Section VII concludes the analysis with general review of the paper contributions.

Manuscript received April 15, 2011. Partially supported by the EC project TUMOR (FP7-ICT-2009.5.4-247754) and by the community initiative program INTERREG III, project "ΥΠΕΡΘΕΝ", financed by the EC through the European Regional Development Fund (ERDF) and by national funds of Greece and Cyprus..

A. Roniotis, V. Sakkalis, K. Marias, and I. Karatzanis are with the Institute of Computer Science, Foundation for Research and Technology, Heraklion, Greece (e-mail: {roniotis; sakkalis; kmarias; karatzan}@ics.forth.gr)

A. Roniotis and M. Zervakis are with the Dept. of Electronic & Computer Engineering, Technical University of Crete, 73100, Chania, Greece (email: roniotis@ics.forth.gr, michalis@display.tuc.gr).

II. Background

Unlike solid tumors, for which simple exponential or geometric expansion represents expansion of tumor volume, the glioma growth rate cannot be determined as the classical doubling rate [1]. Diffusive models use variations of the diffusion – reaction equation (DRE), for simulating the free growth of gliomas [2-5]. They can be used in conjunction with biologically detailed discrete glioblastomas treatment response models [6,7] in order to provide estimates of the response of the non imageable component of the lesion. In order to incorporate the brain tissue heterogeneity (gray and white matter) and the anisotropic migration of tumor cells along white fibers, the most recent models [5, 8] propose the following DRE:

$$\frac{\partial c}{\partial t} = div(\mathbf{D}(\mathbf{x})\nabla c) + f(c) \quad (1)$$

where $c(\mathbf{x}, t)$ is the concentration of glioma cells in position $\mathbf{x}$ at time t, ∇ and div are the gradient and divergence operators respectively. $\mathbf{D}$ is the diffusion tensor, i.e. a matrix of the form:

$$\mathbf{D}(\mathbf{x}) = \begin{vmatrix} D_{11}(\mathbf{x}) & D_{12}(\mathbf{x}) & D_{13}(\mathbf{x}) \\ D_{12}(\mathbf{x}) & D_{22}(\mathbf{x}) & D_{23}(\mathbf{x}) \\ D_{13}(\mathbf{x}) & D_{23}(\mathbf{x}) & D_{33}(\mathbf{x}) \end{vmatrix} \quad (2)$$

where $D_{ij}(\mathbf{x})$, $i, j = 1,2,3$ is the directional local diffusion coefficient used to express the anisotropic migration of cells [5] and $f(c)$ is the net cell proliferation rate. Latest models use

more complex diffusion schemes than (1), such as Eikonal equations [9], but this paper does not work with them. For untreated tumors, variant formalisms of $f(c)$ are proposed [10], with the main ones following either the geometric law:

$$f(c) = \rho c, \tag{3}$$

or Verhulst law:

$$f(c) = \rho c \frac{c_m - c}{c_m} \tag{4}$$

or Gompertz law:

$$f(c) = \rho c \ln \frac{c_m}{c} \tag{5}$$

The term $f(c)$ can also be accustomed to express different proliferation rates related to certain therapeutic schemes. For simulating chemotherapy, $f(c)$ can be determined as:

$$f(c) = \rho c - G(t)c \tag{6}$$

where $G(t)$ is the temporal profile of the chemotherapy treatments, assuming a loss proportional to the strength or amount of therapy at a given time [11]. The chemotherapy term is set to $G(t) = k$ when the chemotherapy is being administered and $G(t) = 0$ otherwise, with k being a measure of effectiveness of chemotherapy. In order therapy to be effective and tumor lesion to decrease in the model, k should exceed ρ.

Finally, the surgical removal (resection) of an accessible tumor is commonly applied, despite low success rates [1]. Resection using diffusive models is simulated by setting the tumor density c to zero inside the resection area at a given time.

Equation (1) is a 2nd order partial differential equation and its solution has to be numerically approximated. The most common numerical methods, being used for developing diffusive models, are Finite Elements Method (FEMs) and Finite Differences Method (FDs). Either explicit or implicit schemes of FEMs and FDs are used for deriving a big linear system, which can be solved by a numerical solver.

Roniotis et al. [12] introduced the mathematical route for implementing diffusive models and presented the direct formalism of the derived linear system, for the common numerical schemes of FDs. The presented framework was designed for three dimensional heterogeneous and anisotropic diffusion focusing on entailing the general form of $f(c)$, so that it could later be adjusted to fit each specific need. The present manuscript not only extends this contribution but also presents a comparative study between different FD and FEM implementations studying accuracy, simulation time, storage consistency and computational consistency, in order to shed light in different computational implementations and identify the optimal selection in view of translating such models into clinical practice. Moreover, different FD schemes are compared according to simulation time, approximation error, effect of grid resolution and time step. Lastly, the paper demonstrates simulations on a real clinical dataset and introduces evaluation metrics of simulation.

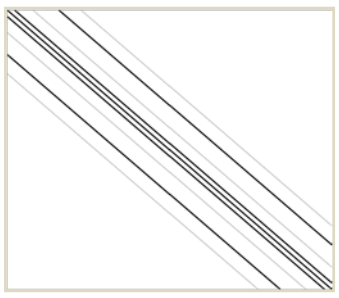

Fig. 1: The sparse Matrix: White areas have zero values, thick lines are 3 diagonals in a row and thin lines are single diagonals.

III. Numerical Methods

The mathematical formulation of the diffusive models is described in this section. Before attempting to formulate a direct expression of the linear system that iteratively solves (1), it is essential to expand it in three dimensions. Suppose that the diffusion tensor at a point $\mathbf{x} = (x_1, x_2, x_3)$ is $\boldsymbol{D}(\mathbf{x})$, then by using the definitions of div and ∇, it becomes:

$$\frac{\partial c}{\partial t} = \sum_{i,j=1}^{3} \frac{\partial^2 c}{\partial x_i \partial x_j} D_{ij} + \sum_{i,j=1}^{3} \frac{\partial c \partial D_{ij}}{\partial x_i \partial x_j} + f(c) \tag{7}$$

The next step is to use Forward Euler (FE), Backward Euler and θ-methods (ΘMs) so as to approximate the solution of (7). These numerical methods are described next.

A. Forward Euler Method (FE)

Assuming that initial and boundary conditions have been defined [4], we study how the explicit method of FE approximates the solution of (7) for a $N_X \times N_Y \times N_Z$ grid. If $c(n\Delta T, i\Delta X, j\Delta Y, k\Delta Z) \equiv C^n_{i,j,k}$, $D_{pq}(i\Delta X, j\Delta Y, k\Delta Z) \equiv D_{pq,i,j,k}$, $i \in \{0, \dots, N_X - 1\}$, $j \in \{0, \dots, N_Y - 1\}$, $k \in \{0, \dots, N_Z - 1\}$ and $p, q \in \{1,2,3\}$, then the partial derivatives of (7) in point $(i\Delta X, j\Delta Y, k\Delta Z)$ can be approximated as:

$$\begin{aligned}
\frac{\partial c}{\partial t} &\to \frac{C^{n+1}_{i,j,k} - C^n_{i,j,k}}{\Delta T} \\
\frac{\partial c}{\partial x} &\to \frac{C^n_{i+1,j,k} - C^n_{i-1,j,k}}{2\Delta X} \\
\frac{\partial^2 c}{\partial x^2} &\to \frac{C^n_{i+1,j,k} - 2C^n_{i,j,k} + C^n_{i-1,j,k}}{\Delta X^2} \\
\frac{\partial^2 c}{\partial x \partial y} &\to \frac{C^n_{i+1,j+1,k} + C^n_{i-1,j-1,k} - C^n_{i+1,j-1,k} - C^n_{i-1,j+1,k}}{4\Delta X \Delta Y} \\
\frac{D_{pq}}{\partial x} &\to \frac{D_{pq,i+1,j,k} - D_{pq,i-1,j,k}}{2\Delta X}
\end{aligned} \tag{8}$$

and similarly for $\frac{\partial c}{\partial y}$, $\frac{\partial c}{\partial z}$, $\frac{\partial^2 c}{\partial y^2}$, and $\frac{D_{pq}}{\partial z}$. Then, by substituting the approximations (8) to (7), we derive:

$$\frac{C^{n+1}_{i,j,k} - C^n_{i,j,k}}{\Delta T} = [A(i,j,k)_0 \quad \dots \quad A(i,j,k)_{18}] \begin{bmatrix} C^n_{i-1,j-1,k} \\ \dots \\ C^n_{i+1,j+1,k} \end{bmatrix} + f\left(C^n_{i,j,k}\right) \tag{9}$$

where

$$\begin{aligned}
A(i,j,k)_2 &= \frac{D_{11,i,j,k}}{\Delta X^2} - \frac{D_{11,i+1,j,k} - D_{11,i-1,j,k}}{4\Delta X^2} \\
&- \frac{D_{21,i,j+1,k} - D_{21,i,j-1,k}}{4\Delta X \Delta Y} - \frac{D_{31,i,j,k+1} - D_{31,i,j,k-1}}{4\Delta X \Delta Z} \\
A(i,j,k)_6 &= \frac{D_{22,i,j,k}}{\Delta Y^2} - \frac{D_{12,i+1,j,k} - D_{12,i-1,j,k}}{4\Delta X \Delta Y} \\
&- \frac{D_{22,i,j+1,k} - D_{22,i,j-1,k}}{4\Delta Y^2} - \frac{D_{32,i,j,k+1} - D_{32,i,j,k-1}}{4\Delta Y \Delta Z} \\
A(i,j,k)_8 &= \frac{D_{33,i,j,k}}{\Delta Z^2} - \frac{D_{13,i+1,j,k} - D_{13,i-1,j,k}}{4\Delta X \Delta Z} \\
&- \frac{D_{23,i,j+1,k} - D_{23,i,j-1,k}}{4\Delta Y \Delta Z} - \frac{D_{33,i,j,k+1} - D_{33,i,j,k-1}}{4\Delta Z^2} \\
A(i,j,k)_{10} &= \frac{D_{33,i,j,k}}{\Delta Z^2} + \frac{D_{13,i+1,j,k} - D_{13,i-1,j,k}}{4\Delta X \Delta Z} \\
A(i,j,k)_{12} &= \frac{D_{22,i,j,k}}{\Delta Y^2} + \frac{D_{12,i+1,j,k} - D_{12,i-1,j,k}}{4\Delta X \Delta Y} \\
A(i,j,k)_{16} &= \frac{D_{11,i,j,k}}{\Delta X^2} + \frac{D_{11,i+1,j,k} - D_{11,i-1,j,k}}{4\Delta X^2}
\end{aligned}$$

$$A(i,j,k)_0 = -A(i,j,k)_4 = -A(i,j,k)_{14} = A(i,j,k)_{18} = \frac{D_{12,i,j,k}}{2\Delta X \Delta Y}$$
$$A(i,j,k)_1 = -A(i,j,k)_3 = -A(i,j,k)_{15} = A(i,j,k)_{17} = \frac{D_{13,i,j,k}}{2\Delta X \Delta Z}$$
$$A(i,j,k)_5 = -A(i,j,k)_7 = -A(i,j,k)_{11} = A(i,j,k)_{13} = \frac{D_{23,i,j,k}}{2\Delta Y \Delta Z}$$
$$A(i,j,k)_9 = -2\frac{D_{11,i,j,k}}{\Delta X^2} - 2\frac{D_{22,i,j,k}}{\Delta Y^2} - 2\frac{D_{33,i,j,k}}{\Delta Z^2} \quad (10)$$

If we vectorize $C^n_{i,j,k}$ at time mΔT as:

$$\mathbf{C}^{\mathrm{m}} \equiv \left[\underbrace{C^m_{0,0,0} \quad C^m_{0,0,1} \quad \dots \quad C^m_{0,1,0} \quad \dots \quad C^m_{N_X-1,N_Y-1,N_Z-1}}_{N_X N_Y N_Z}\right]^T \quad (11)$$

then, the overall solution of the equation at time $n+1$, for given $\mathbf{C}^0$, can be found by iteratively solving $\frac{\mathbf{C}^{n+1}-\mathbf{C}^{\mathrm{n}}}{\Delta T} = \mathbf{A}\mathbf{C}^{\mathrm{n}} + F(\mathbf{C}^{\mathrm{n}})$ where $\mathbf{A}$ is a $N_X N_Y N_Z \times N_X N_Y N_Z$ 19-diagonal matrix with its elements defined as:

$$\mathrm{A}_{ml} = \begin{cases} A(i,j,k)_0, l = m - N_Y N_Z - N_Z & A(i,j,k)_{10}, l = m+1 \\ A(i,j,k)_1, l = m - N_Y N_Z - 1 & A(i,j,k)_{11}, l = m + N_Z - 1 \\ A(i,j,k)_2, l = m - N_Y N_Z & A(i,j,k)_{12}, l = m + N_Z \\ A(i,j,k)_3, l = m - N_Y N_Z + 1 & A(i,j,k)_{13}, l = m + N_Z + 1 \\ A(i,j,k)_4, l = m - N_Y N_Z + N_Z & A(i,j,k)_{14}, l = m + N_Y N_Z - N_Z \\ A(i,j,k)_5, l = m - N_Z - 1 & A(i,j,k)_{15}, l = m + N_Y N_Z - 1 \\ A(i,j,k)_6, l = m - N_Z & A(i,j,k)_{16}, l = m + N_Y N_Z \\ A(i,j,k)_7, l = m - N_Z + 1 & A(i,j,k)_{17}, l = m + N_Y N_Z + 1 \\ A(i,j,k)_8, l = m - 1 & A(i,j,k)_{18}, l = m + N_Y N_Z + N_Z \\ A(i,j,k)_9, l = m & 0, otherwise \end{cases}$$

where:

$$m = iN_Y N_Z + jN_Z + k \text{ and } m, l \in \{0, \dots, N_X N_Y N_Z - 1\} \quad (12)$$

and F is the *vectorization operator* defined as:

$$F(\boldsymbol{C}^n) \equiv \left[f(C^n_{0,0,0}) \quad f(C^n_{0,0,1}) \quad \dots \quad f(C^n_{N_X-1,N_Y-1,N_Z-1})\right]^T \quad (13)$$

After having acquired the $\mathbf{A}$ matrix, a direct solution can be found directly by calculating:

$$\mathbf{C}^{n+1} = (\mathbf{I} + \Delta T \mathbf{A})\mathbf{C}^{\mathrm{n}} + \Delta T \cdot F(\mathbf{C}^{\mathrm{n}}) \quad (14)$$

where $\mathbf{I}$ is the $N_X N_Y N_Z \times N_X N_Y N_Z$ identity matrix. This is the result of the forward Euler method that is called *forward* due to the *direct* estimation of (14). However, the main issue when using this method is numerical stability. As proven in [13], in order this method to stable the following condition must hold:

$$\Delta T \leq min_{x,y,z}\left(\frac{1}{2}\frac{1}{\frac{D_{11}(x,y,z)}{\Delta X^2} + \frac{D_{22}(x,y,z)}{\Delta Y^2} + \frac{D_{33}(x,y,z)}{\Delta Z^2}}\right) \quad (15)$$

B. Backward Euler (BE)

Similarly to FE, for the implicit method of BE we derive:

$$(\mathbf{I} - \Delta T \mathbf{A})\mathbf{C}^{n+1} - \Delta T \cdot F(\mathbf{C}^{\mathrm{n+1}}) = \mathbf{C}^{\mathrm{n}} \quad (16)$$

TABLE I
VECTORIZATION OPERATOR FOR DIFFERENT PROLIFERATION RATES

Proliferation Rate	Constant Rate *f(c)*	Vectorization Operator $F(\mathbf{C}^{\mathrm{n}})$
Exponential	ρc	$\rho \boldsymbol{C}^n$
Verhulst (logistic)	$\rho c \frac{c_m - c}{c_m}$	$\frac{\rho}{c_m} diag(\boldsymbol{C}^n)(c_m \mathbf{1}^{1\times N_X N_Y N_Z} - \boldsymbol{C}^n)$
Gompertz	$\rho c \ln\frac{c}{c_m}$	$\rho diag\left(ln(c_m \mathbf{1}^{1\times N_X N_Y N_Z}) - ln(\boldsymbol{C}^n)\right)\boldsymbol{C}^n$
Chemotherapy	$\rho c - G(t)c$	$\begin{cases}(\rho - k)\boldsymbol{C}^n & , chemo\ at\ time\ n\Delta T \\ 0 & , otherwise\end{cases}$

$$diag\begin{bmatrix}x_1\\x_2\\\dots\\x_N\end{bmatrix} = \begin{bmatrix}x_1 & 0 & \dots & 0\\0 & x_2 & & 0\\\dots & \dots & \dots & \dots\\0 & 0 & \dots & x_N\end{bmatrix} \qquad \mathbf{1}^{1\times N} = \left.\begin{bmatrix}1\\1\\\dots\\1\\1\end{bmatrix}\right\} N$$

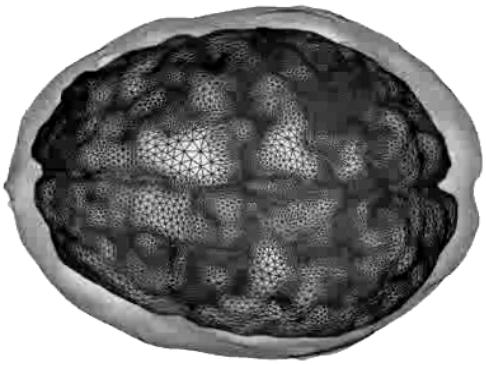

Fig. 2. An example of meshing 3-dimensional brain using Lagrange Quadratic elements for mesh generation.

where $\mathbf{A}$ is the same matrix of (12). The emerging system is large and can be expressed with a symmetric, positive definite matrix, thus an iterative method for solving linear systems, such as the conjugate gradient method can be used. Unconditional stability and accuracy are the main advantages of BE, in contrary to the increased computational load [14].

C. θ-methods (ΘMs) / Crank Nikolson (CN)

The ΘMs use a balancing parameter $\theta \in [0,1]$, so as to combine implicit and explicit numerical schemes concurrently. By using ΘMs, the system changes to $(\mathbf{I} - \theta\Delta T\mathbf{A})\mathbf{C}^{n+1} - \theta\Delta T \cdot F(\mathbf{C}^{\mathbf{n+1}}) = (\mathbf{I} + q\Delta T\mathbf{A})\mathbf{C}^n + q\Delta T \cdot F(\mathbf{C}^{\mathrm{n}})$ where $q = 1 - \theta$. As in BE, a method for solving linear systems is required. The ΘMs are flexible due to choice of parameter θ but higher computational and storage load are required [14]. Crank Nikolson is a θ-method for θ=½.

D. Proliferation rate

The proliferation rate of the implemented model can be adjusted in the described framework by manipulating the operator F, according to equation (13). Table I presents the emerging F for the different proliferation schemes decribed by equations (3),(4)(5) and (6).

IV. IMPLEMENTATION METHODS

A. Finite Differences

The diffusive model, the mathematical formulation of which has been described in the previous section, has been implemented in C++. The derived big sparse matrix $\mathbf{A}$ has been stored by using the row-indexed sparse storage mode [14]. Fig. 1 presents the shape of the tridiagonal $\mathbf{A}$ with fringes. Lastly, in order to solve the derived systems for BE and ΘMs., the biconjugate gradient method has been used.

B. Finite Elements

The diffusive model has also been implemented with the Finite Element Method (FEM), using commercial software (COMSOL), in order to compare it's efficiency to that of the FD model. The model uses tetrahedral Lagrange Quadratic Elements. In Fig. 2, an example of a meshed brain using FEs is presented.

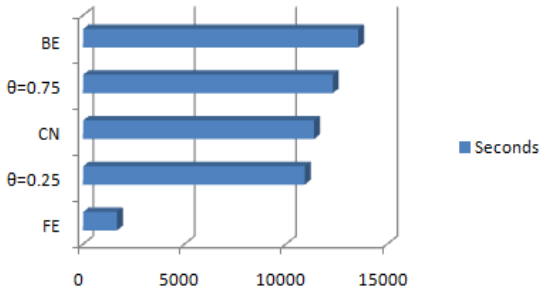

Fig. 3. Simulation time for the five different schemes

Like FDs, the solution requires the construction of a large sparse matrix, having its elements randomly located. Biconjugate gradient methods can be used for the solver, but the rate of convergence is slow and the quality of the approximate solution may be sensitive to roundoff errors [15]. Thus, there are limitations in the dimensions of the emerging sparse matrix

C. *Preparation of Experiments and Testing Procedure*

In order to study the performance of the different methods that have been developed, a simplified test case of the pure diffusion equation is used for which there is a known analytical continuous expression of the solution. Hence, the magnitude of the deviation of the method from the real solution can be calculated.

We assume that tumor cell concentration $c(\mathbf{x}, t)$ follows the pure diffusion equation:

$$\frac{\partial c}{\partial t} = div(\mathrm{D(x)}\nabla c) + f(c) \qquad (17)$$

where D is a uniform diffusion coefficient and the net proliferation term $f(c)$ is zero. If we set the initial concentration c_0 inside a sphere of radius a and zero outside this sphere, then, due to symmetry and isotropic diffusion, the concentration of glioma depends only on the distance from the center of the sphere r. The concentration at time t is given by the expression [16]:

$$C(r,t) = \frac{1}{2}c_0\left(erf\left(\frac{a-r}{2\sqrt{Dt}}\right) + erf\left(\frac{a+r}{2\sqrt{Dt}}\right)\right) - \frac{c_0}{r}\sqrt{\frac{Dt}{\pi}}\left(exp\left(-\frac{(a-r)^2}{4Dt}\right) - exp\left(-\frac{(a+r)^2}{4Dt}\right)\right) \qquad (18)$$

For the FD model we have used the parameters: $f(c) = 0$, $D = 0.5 \;\; mm^2/day$, $a = 10\,mm$, $\Delta X = \Delta Y = \Delta Z \equiv \Delta = 1\,mm$, $\Delta T = 0.25\,days$, $N_X = N_Y = N_Z = 128 \equiv N$ points

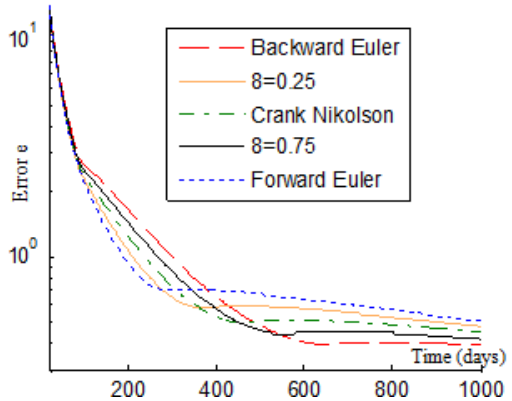

Fig. 4. Logarithmic visualization of error e in time (days)

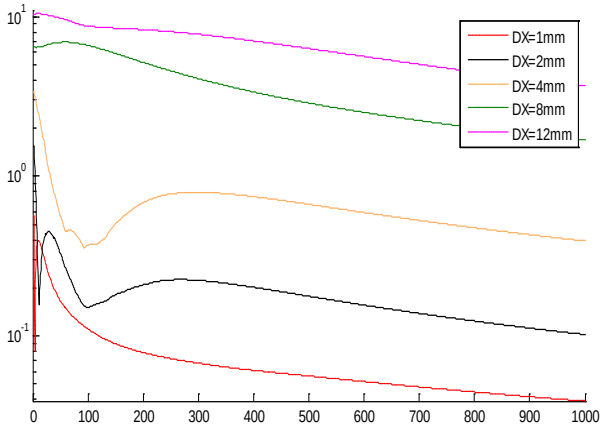

Fig. 5. Logarithmic graph of error e (y-axis) according to time (x-axis). The graph is plotted for five different grid resolutions, applied for 1000 fictitious days

and $c_0 = 10^4\ cells/mm^3$. Five different simulations were run for 1000 fictitious days, using FE, three ΘMs for θ=0.25, θ=0.5 (CN), θ=0.75, and BE performed on a Pentium 4 at 3.8 GHz.

V. Analysis On Finite Differences

A. *Simulation Time*

The five different experiments that have been applied were run for 1000 fictitious days. Fig. 3 shows the simulation time of each experiment, in seconds. The simulation times for FE, θ=0.25, CN, θ=0.75 and BE are 27'53", 182'13", 190'1", 205'16" and 226'11" respectively. Thus, if there is urgent need for low simulation time, one could use FE, since it is 8.07 times faster than BE. However, there is a tradeoff between accuracy and execution speed, as will be observed later.

B. *Approximation Error*

In order to estimate the approximation error of each scheme, the normalized mean absolute error e is introduced. Due to symmetry, e at time $t = n\Delta T$ is computed as

$$e = \frac{1}{N}\sum_{i=1}^{N}\left|\frac{C(i\Delta X, n\Delta T) - C^n_{i,\frac{N}{2},\frac{N}{2}}}{c_0}\right| \times 100\% \qquad (19)$$

Fig. 4 presents the logarithmic graph of e in time for each scheme. It is noticeable that all schemes initially produce high errors, with the best performance carried by FE with e =12%. A possible explanation is that the initial concentration $C(r,0)$ has an abrupt step descent at $r = 10mm$. This makes the approximation of the local partial derivatives at the edge of this step erroneous for all schemes. However, as simulation continues, e tends to significantly decrease for all schemes.

Continuing, one can observe that e decreases to values less than 1% for all schemes on day 190, 203, 252, 287 and 308 for FE, 0.25-method, CN, 0.75-method and BE, respectively. Generally, it is noticeable that the smoother one scheme decreases at the beginning, the better performance it achieves at the end. Indeed, the BE method starts with the smoothest decrease, but eventually yields the lowest error, 0.39%. After some time, error reaches balancing values for all schemes.

BE yields the most accurate approximations of $C(r,t)$, but with increasing simulation times, as seen in Fig.3. If there is need for proximate simulation time, one could use some faster modeling schemes, such as CN, since the error is still below 0.45%. It is observed here that there is a tradeoff between

accuracy and execution speed, since the faster the method is, the higher error e it yields

C. *Effect of grid resolution*

In order to study the effect of grid resolution in simulation accuracy, five different grids have been used for approximating equation (18) in a cubic space of 120x120x120mm, by using the Backward Euler scheme. The different grids have used $\Delta = 1mm, 2mm, 4mm, 8mm$ and $12mm$ respectively. Fig 5 presents the logarithmic graph of the error e in the first 1000 fictitious days.

As expected, the lowest e occurs for $\Delta = 1mm$ and does not overcome 0.04%. As Δ increases, error e increases. For $\Delta = 2, 4, 8$ and $12mm$ the lowest error is 0.10%, 0.39%, 1.69% and 3.67% respectively. Doubling the grid element size from $\Delta = 1mm$ to $2mm$ yields a 157% increase in mean e. Similarly, by doubling from $2mm$ to $4mm$, mean e increases 250%. Lastly, doubling from $4mm$ to $8mm$ results in a 453% increase in mean error. This means that the error rises more rapidly as the grid resolution decreases.

D. *Effect of time step*

It is important to check the effect of time step ΔT in simulation accuracy. The experiment studied the performance of the three basic numerical schemes, namely FE, CN and BE for approximating the concentration of cells for 1000 fictitious days. The spatial step Δ was set to 1mm.

In Figure 6 we present the logarithmic graph of the mean error e ($\bar{e}$) for the 1000 days of simulation. The minimum $\bar{e}$ is 0.0888%, performed by the CN scheme for $\Delta T = 2$ days. The minimum $\bar{e}$ for FE and BE is 0.79% and 1.01% higher than that of CN, respectively. Moreover, for ΔT=0.001 and ΔT=0.01, the errors for all schemes remain unchanged. Especially for FE, this holds for ΔT values from 0.001 to 0.1. This indicates that there is a balancing value for ΔT under which no more accuracy can be achieved. In our experiment, this balancing value of ΔT is 0.1 for the FE method and 0.01 for CN and FE.

As expected, the error generally increases as ΔT increases, for all schemes. For Forward Euler, $\bar{e}$ increases with ΔT, but when ΔT changes from 1 to 1.5 days, a slight decrease of 1.4% is observed. ΔT=1.5 days is the threshold, over which FE is instable. For BE, $\bar{e}$ increases smoothly as ΔT increases, with a small decrease of 3.38% from ΔT=0.5 to 1 days. $\bar{e}$ for the Crank Nikolson scheme shows a basin-like behavior, since it starts at 0.0897% for ΔT=0.001, rises smoothly to 0.0984% for ΔT=0.5, falls at 0.0888% at ΔT=1 and gradually increases from there on.

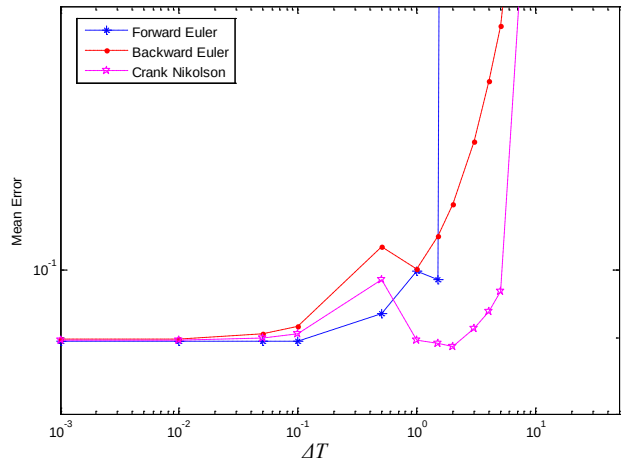

Fig. 6. Mean error $\bar{e}$ for changing ΔT, using FE, CN and BE. The mean error has been calculated for 1000 fictitious days.

TABLE II
ERROR $\bar{E}$ AFTER 1000 DAYS FOR DIFFERENT GRID RESOLUTIONS

Scheme	125.000	166.375	216.000	343.000
Finite Elements	**2.97%**	**0.16%**	**0.06%**	**-**
Backward Euler	**2.99%**	**0.15%**	**0.06%**	**0.04%**
Forward Euler	**4.09%**	**0.21%**	**0.10%**	**0.08%**
Crank Nikolson	**3.16%**	**0.17%**	**0.08%**	**0.07%**

CN scheme yields the lowest $\bar{e}$ for higher ΔT. CN for $\Delta T = 4$ has almost the same accuracy with the respective case for $\Delta T = 0.1$ of BE. Similarly, CN has the same accuracy with the FE scheme for $\Delta T = 0.5$. Thus a time step 40 times bigger than that of BE yields equivalent accuracy for CN. For smaller time steps (around 0.1 days), FE yields the lowest $\bar{e}$.

VI. COMPARISON WITH FINITE ELEMENTS

Both Finite Differences and Finite Elements have been used for developing diffusive models. However, the comparison of the two schemes on the implementation of the diffusive model and/or the justification of each choice is still unclear issue.

FEMs and FDs have been compared at approximating equation (18) on the same sphere presented earlier. Four different experiments have been performed for different grid resolutions, with the FEMs having used 125.000, 166.375, 216.000 and 343.000 elements, respectively. For the same experiments, FDs have used the same number of cubic elements (voxels). When designing a model, developers should not ignore the computational limitations of the model. The process power and storage capacity of the computers that are used in clinical practice should be taken into account, since a resource-demanding model would turn out to be cumbersome when no access to supercomputers is possible. The above comparison issues are elaborated in the following.

A. *Accuracy*

The accuracy of the models has been studied, by estimating the deviation of the approximated solution $C_{appr}(r,t)$ from the real solution $C(r,t)$. The error E of the approximation at a distance r from the center of the sphere, is estimated as:

$$E(r) = \left|C_{appr}(r,t) - C(r,t)\right| \quad (20)$$

where t is set to 1000 days. The accuracy of the models is estimated by calculating the mean normalized error $\bar{E}$ as

TABLE III
SIMULATION TIME FOR DIFFERENT GRID RESOLUTIONS

Scheme	125.000	166.375	216.000	343.000
Finite Elements	**31”**	**20’ 12”**	**151’ 3”**	**-**
Backward Euler	**6”**	**7’ 12”**	**78’ 5”**	**210’ 25”**
Forward Euler	**1”**	**23”**	**5’ 32”**	**35’ 48”**
Crank Nikolson	**6”**	**6’ 59”**	**64’1”**	**198’ 12”**

follows:

$$\bar{E} = \frac{1}{\Delta}\int_{r=0}^{\Delta} E(r) \times 100\% \quad (21)$$

Table II presents the comparative results of approximating the pure diffusion equation with Lagrange Quadratic FEMs, FE, CN and BE. The rows present the total number of elements of the mesh. The columns present the mean error of approximation at the 1000th day of diffusion simulation for each model.

In the first case (125.000 elements), FEMs achieved slightly lower error than that of Backward Euler and lower than Forward Euler. For 166.375 elements, FEMs produced higher error than Backward Euler and lower than Forward Euler. For 216.000 elements, Finite Elements produced the same error with Backward Euler and lower than Forward Euler. Lastly, for 343.000 elements, FEs caused memory overflow and could not approximate the solution. On the other hand, Backward Euler produced the lowest error, at 0.04%.

B. Simulation Time

Table III presents the simulation time of each of the previous experiments, dependant on the grid resolution. It is observed that simulation time FEMs in the first experiment (125.000 elements) is 5.16 times higher than BE and 31 times higher than FE. In the second case, simulation time for FEMs is 2.8 times higher than BE and 52.69 times higher than FE. Lastly, in the third case, FEMs has 1.93 times higher simulation time than BE and 27.2 times higher than FE.

C. Storage and Computational Consistency

One important issue governing the comparison of the models that have been implemented with FEMs and FDs, is their computational consistency. If the grid resolution of the mesh exceeds some limits, then the storage of the sparse matrix and the solving of the solution are practically impossible [14]. This is important, since a developer of such a system should bear in mind that clinicians may not have access to supercomputers or grid services, thus they have to adjust their products to realistic conditions.

In this experiment, different grid resolutions have been used for approximating equation (18). In Fig. 7, we present the maximum element number that the computer used in the experiment, without memory overflow. As observed in the chart, FEM "crashes" with total element number being almost

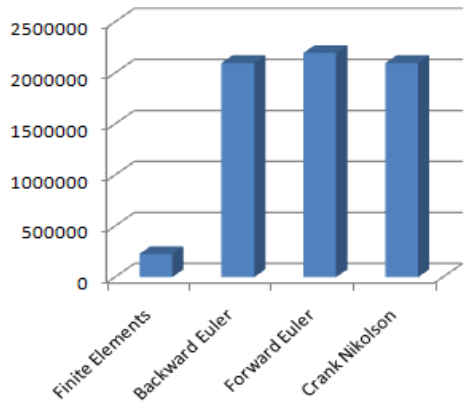

Fig. 7: The maximum number of elements, for which no memory overflow is performed.

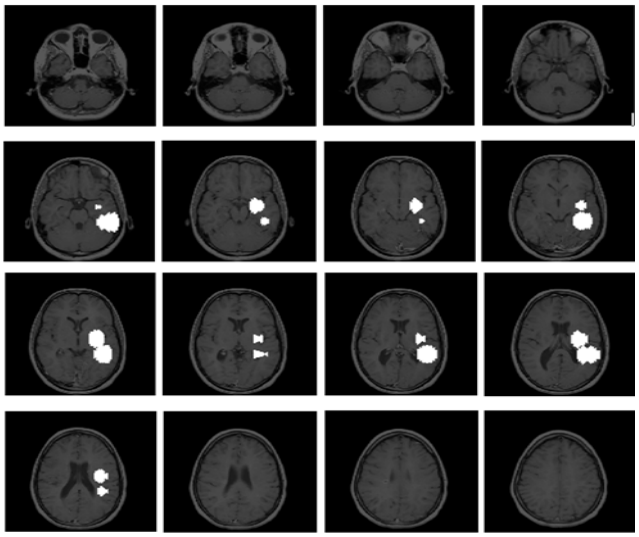

Fig. 8. 16 MRI slices (out of 27) with glioma in advanced stage. White areas are the tumor areas as delineated by the clinician.

10% of the respective number of FD models.

D. Experimental Results on a Clinical Case

FEMs are often preferred by engineers, since they allow considerable freedom in locating computational elements. This is important when dealing with highly irregular geometries. However, in the case of diffusive models, as in glioma models, the previous experiments show that the application of FEMs does not add improvement in the overall accuracy of the model. Indeed, FEMs achieve similar results in terms of accuracy with FDs. On the other hand, FDs require less simulation time and can extend the limitation of the total element number to 10 times more than the number of FEMs. Moreover, the previous analysis implies that BE is expected to achieve the highest scores, in terms of accuracy, for the approximation of the DRE.

Therefore, we select BE for further applying the model to a real clinical case. Fig. 8 presents a series of 16 MRI slices (out of 27) of a 58 year old patient, taken from the Harvard Medical School database [17], with white areas reflecting glioblastoma

Fig. 9. 3D representation of MRI images: (left column) Initial Data, (central column) Simulated data after 112 days, by using BE and (right column) Real data on 112th day

multiforme, being delineated by a clinician. The patient passed away after 112 days and no therapy was applied, because of the advanced stage of the tumor at the time of diagnosis.

The geometrical proliferation rate ρ was set, according to [10], at $\rho = 0.012\ \text{day}^{-1}$. Moreover, $D_{ij}(\mathbf{x})$ was set to $w_i(\mathbf{x})D(\mathbf{x})$ for $i = j$ and zero otherwise, where $w_i(\mathbf{x}) \in [0,1]$ expresses the local anisotropic migration of cells along the direction i (x, y or z axis) and $D(\mathbf{x})$ is the local diffusion coefficient. $D(\mathbf{x})$ equals $D_g = 0.13mm^2/day$, when point $\mathbf{x}$ is located in gray matter and $D_w = 0.65mm^2/day$, when in white matter. Furthermore, local anisotropy parameter $w_i(\mathbf{x})$ was estimated according to [18, 19], the initial concentration was defined at $200cells/mm^3$ and the density threshold for detection at $400cells/mm^3$. Lastly, the grid distances $\Delta X, \Delta Y$ and ΔZ were defined at $1mm$, $1mm$ and $3mm$ respectively, time step was defined at 0.5 days and overall simulation time at 112 days, when the patient passed away. Fig. 9 (left column), presents the 3D visualization of the MRI images of Fig. 8 at the time of diagnosis taken from different angles. The central column presents the respective results of the simulation after 112 days. The last column presents the actual MRI data after 112 days.

In order to make a quantitative evaluation of the agreement between the simulated tumor and the final tumor (taken as ground truth), Jaccard (JC), Dice (DS) and Volume Similarity (VS) metrics are used [20,21]. JC, DS and VS are defined as:

$$\begin{aligned} \text{JC} &= \text{TP}/\ (\text{FP}+\text{TP}+\text{FN}) \\ \text{DS} &= 2\text{TP}/\ (\text{FP}+2\text{TP}+\text{FN}) \\ \text{VS} &= 1-|\text{FP}-\text{FN}|/(\text{FP}+2\text{TP}+\text{FN}) \end{aligned} \tag{22}$$

TP is the number of tumor voxels belonging to both the ground truth and simulated result, FP is the number of tumor voxels belonging to simulated result but not belonging to ground truth and FN is the number of tumor voxels belonging to ground truth but not belonging to simulated tumor. In this case, TP, FP and FN are 8515, 356 and 299 voxels, respectively. Thus, the metrics are JC=92.86%, DS=96.30% and VS=99.68%.

VII. Discussion & Conclusion

When designing a model, engineers should not ignore the computational limitations of the model. The processing power and storage capacity of the computers that are used in clinical practice should be seriously taken into account, since a resource-demanding model would turn out to be cumbersome when no access to supercomputers is possible. This paper stresses the limitations and advantages of each modeling scheme and provides quantitative proof. Hence, engineers and bioinformaticians working with glioma models (or any model with similar diffusion – reaction behavior) could assess the limitations of the model that they are about to develop, especially for real clinical models. Therefore, even if one method (e.g. FEMs) would initially seem as the most accurate, this paper indicates specific tradeoffs (such as simulation time, storage and computational needs) that can cause computational problems on the main-stream computers of hospitals and may alter the preference to this method.

By comparing different schemes of FDs, we conclude that Explicit methods (FE) run faster, but are prone to errors. On the other hand, implicit methods (BE, CN, θ-methods) produce lower errors, but are computationally greedy. Especially, BE has performed the most accurate approximation of the real solution, but also results in the worst simulation time. Moreover, the error increases rapidly as the grid resolution decreases. Finally, FE yields good approximation for small simulation time steps ΔT, but CN yields the low error for higher values of ΔT.

By comparing FDs with FEMs, it is observed that FEMs do not provide additional accuracy to the model. On the other hand, FDs need less simulation time and extend the limitation of the total element number to almost 10 times more than the number of FEs. This extends the accuracy potentials of FDs into higher levels, because FDs can use higher resolution than FEMs.

In this paper we develop a complete and practical study for the mathematical solving of the diffusion - reaction equation, used for simulating either glioma growth or other diffusive phenomena. Moreover, a qualitative analysis on different numerical schemes of FDs and FEMs is presented, using a simplified test case. This analysis indicates that FDs are practically more suitable for the needs of a glioma diffusive model. The application of a diffusive model on a real dataset produced a realistic approximation of the growth tumor. The models, however, need to be validated more extensively on larger glioma datasets.

References

[1] F. G. Blakenberg, R. L. Teplitz, W. Ellis, M. S. Salamat, B. H. Min, L. Hall, et al. "The influence of volumetric tumor doubling time, DNA ploidy, and histologic grade on the survival of patients with interracial astrocytomas," *AJNR Am. J. NeuroRad.,* vol. 16, pp. 1001-12, 1995.

[2] P. Tracqui, "From passive diffusion to active cellular migration in mathematical models of tumor invasion," *Acta Bibliotheoretica*, vol. 43, pp 443-464, 1995.

[3] K. R. Swanson, E. C. Alvord, and J. D. Murray, "A Quantitative Model for Differential Motility of Gliomas in Grey and White Matter," *Cell Proliferation.*, vol. 33, no. 5, pp. 317-330, 2000.

[4] S. Jbabdi, E. Mandonnet, and H. Duffau, "Simulation of anisotropic growth of low-grade gliomas using diffusion tensor imaging," *Magn. Reson. Med.*, vol. 54, pp. 616-24, 2005.

[5] O. Clatz, M. Sermesant, P. Bondiau, H. Delingette, S. K. Warfield, G. Malandain, and N. Ayache, "Realistic simulation of the 3-D growth of brain tumours in MR images coupling diffusion with biomechanical deformation," *IEEE Transactions on Medical Imaging*, vol. 24, pp. 1334-1346, 2005.

[6] D. Dionysiou, G. S. Stamatakos, N. Uzunoglu, K. Nikita, and A. Marioli, "A four-dimensional simulation model of tumour response to radiotherapy in vivo: parametric validation considering radiosensitivity, genetic profile and fractionation", *J Theor Biol*, vol. 230, pp. 1-20, 2004.

[7] G. S. Stamatakos, V. Antipas, and N. Uzunoglu, "A spatiotemporal, patient individualized simulation model of solid tumor response to chemotherapy in vivo: the paradigm of glioblastoma multiforme treated by temozolomide", *IEEE Tr Biom Eng*, vol. 53, no. 8, pp. 1467-77, 2006.

[8] R. Sodt, R. Rockne, K.R. Swanson, I. Kalet, "Simulation of Anisotropic Growth of Gliomas Using Diffusion Tensor Imaging," *Int. Conf. on Mathem. Biol. and Annual Meeting Society for Math. Biol.*, University of British Columbia, Vancouver, July 2009.

[9] E. Konukoglu, O. Clatz, B. H. Menze, M. A. Weber, B. Stieltjes, E. Mandonnet, H. Delingette, and N. Ayache, "Image Guided Personalization of Reaction Diffusion Type Tumor Growth Models using Modified Anisotropic Eikonal Equations", *IEEE Tr M Imag*, vol. 27, pp. 73-95, 2009

[10] M. Marusic, Z. Bajzer, J. P. Freyer, and S. Vuk-Palovic, "Analysis of growth of multicellular tumour spheroids by mathematical models," *Cell Prolif*, vol. 27, pp. 73-94, 1994.

[11] K. R. Swanson, E. C. Alvord Jr., J. D. Murray, "Quantifying Efficacy of Chemotherapy of Brain Tumors (Gliomas) with Homogeneous and

Heterogeneous Drug Delivery," *Acta Biotheoretica*, vol. 50, no. 4, pp. 223-237, 2002.
[12] A. Roniotis, K. Marias, V.Sakkalis, G. Tsibidis, and M. Zervakis, "A Complete Mathematical Study of a 3D Model of Heterogeneous and Anisotropic Glioma Evolution," *IEEE Eng in Med and BiolSocConf*,vol. 1, pp. 2807-2810, 2009.
[13] S. Puwal, and B. J. Roth, "Forward Euler Stability of the Bidomain Model of Cardiac Tissue," *IEEE Tr Biom Eng.*, vol. 54, no. 5, pp. 951-953, 2005.
[14] S. Teukolsky, W. Vetterling, and B. Flannery, "Numerical Recipes: The Art of Scientific Computing (Third Edition)," Cambridge University Press, NY, 2007.
[15] Y. Saad, "Iterative methods for sparse linear systems (2nd ed.)", S.I.A.M., Philadelphia, 2003.
[16] J. Crank, "The Mathematics of Diffusion (Second Edition)," Oxford University Press, NY, 1975.
[17] Harvard Medical School, "The Whole Atlas Brain", Available: http://www.med.harvard.edu/AANLIB/home.html [Accessed: Dec. 14, 2008].
[18] R. A. Bammer, M. E. Moseley ME, "In vivo MR tractography using diffusion imaging," *Eur J Radiol*, vol. 45, pp. 223-234, 2002.
[19] T. Rohlfing, N. M. Zahr, E. V. Sullivan, and A. Pfefferbaum, "The SRI24 multichannel atlas of normal adult human brain structure," *Human Brain Mapping*, vol. 31, no. 5, pp. 798-819, 2010.
[20] R. Cárdenes, M. Bach, Y. Chi, I. Marras, R. Luis, M. Andersson, P. Cashman, and M. Bultelle, "Multimodal evaluation for medical image segmentation", *CAIP 2007*, pp. 229-236, 2007.
[21] A. Roniotis, G. Manikis, V. Sakkalis, M. Zervakis, I. Karatzanis, and K. Marias, "High grade glioma diffusive modeling using statistical tissue information and diffusion tensors extracted from atlases," *IEEE Trans Inform. Tech. in Biom 2012 (in press)*, doi: 10.1109/TITB.2011.2171190

Alexandros Roniotis is a Ph.D. candidate in the Dept of Electronics and Computer Engineering in the Technical University of Crete. In 2006 he completed his BSc in Informatics and Telecommunications in University of Athens, Greece, and took his M.Sc. in Signal Processing and Communications, Electrical & Electronic Engineering Dept of Imperial College London, UK, in 2007. Since 2008 he works in the Institute of Computer Science - Foundation for Research and Technology (ICS - FORTH), Greece. His research interests include modeling of biological processes; biomedical imaging, digital image processing and pattern recognition.

Vangelis Sakkalis holds a Ph.D. in Electronics and Computer Engineering from the Technical University of Crete. Previously he completed his Masters in Engineering and Physical Science in Medicine at Imperial College of Science, Technology and Medicine, UK. He holds an Associate Researcher position in the Institute of Computer Science – Foundation for Research and Technology (ICS - FORTH). His background falls in Computational Medicine, Biomedical Engineering, Atomic-Molecular Physics, Optoelectronics and Laser. His research interests include biosignal and image analysis, visualization, classification algorithms, biostatistics and biomedical informatics and modeling.

Ioannis Karatzanis holds a BSc in Physics from the University of Crete. He is a member of the technical team of the Computational Medicine Laboratory in the Institute of Computer Science of the Foundation for Research and Technology – Hellas (CML - ICS - FORTH), where he is involved in the development of user interfaces for medical applications (both for clinical environment and for home environment), Digital Image Processing, Signal Processing and Analysis, and many more...

Michalis E. Zervakis holds a Ph.D degree in Electrical Engineering from the University of Toronto, Canada, since 1990. He joined the Technical University of Crete on January 1995, where he is serving as Professor at the department of Electronic and Computer Engineering. He served as Associate Editor in the "IEEE Transactions on Signal Processing" from 1994 to 1996. He was an assistant professor with the University of Minnesota-Duluth, USA, from September 1990 to December 1994.Prof. Zervakis is the director of the Digital Image and Signal Processing Laboratory (DISPLAY) at the Technical University of Crete. Under his direction, the lab is involved in research on modern aspects of signal processing, including estimation and constrained optimization, multi-channel and multi-band signal processing, wavelet analysis for data/ image processing and compression, neural networks and fuzzy logic with applications in biomedical data analysis, imaging systems and integrated automation systems. Developments also include DSP-based real-time implementation.

Dr. Kostas Marias holds a Principal Researcher position in the Institute of Computer Science (ICS - FORTH), leading the Computational Medicine Laboratory (CML). During 2001 - 2003, he worked as a Researcher at the University of Oxford after completing his PhD in the field of Medical Image Analysis. He also holds an MSc degree from Imperial College of Science, Technology and Medicine in Physical Science and Engineering in Medicine as well as an Electrical Engineering Diploma from the National Technical University of Athens (N.T.U.A). His current research interests are in the areas of medical image analysis, registration and fusion and cancer modeling. He is member of IEEE since 2003.